Optical emissivity study of the critical fluctuations in mercury wetting film on sapphire

2003 J. Phys.: Condens. Matter 15 6179

(http://iopscience.iop.org/0953-8984/15/36/308)

INSTITUTE OF PHYSICS PUBLISHING JOURNAL OF PHYSICS: CONDENSED MATTER

J. Phys.: Condens. Matter **15** (2003) 6179–6198 PII: S0953-8984(03)60532-1

Optical emissivity study of the critical fluctuations in mercury wetting film on sapphire

Y Kajihara, Y Ohmasa and M Yao[1]

Department of Physics, Graduate School of Science, Kyoto University, Kyoto 606-8502, Japan

E-mail: yao@scphys.kyoto-u.ac.jp

Received 4 March 2003, in final form 9 July 2003
Published 29 August 2003
Online at stacks.iop.org/JPhysCM/15/6179

Abstract

The thermal radiation intensity from the mercury/sapphire interface shows an anomalous decrease in the prewetting supercritical region (Ohmasa *et al* 2000 *J. Phys.: Condens. Matter* **12** A375). This anomaly is a clear indication of the optical diffuse scattering caused by the critical fluctuations in the mercury wetting film formed on the sapphire substrate. In the present work, we measured the thermal radiation spectrum in the wavelength range $500 \lesssim \lambda < 1650$ nm, and deduced the diffuse scattering intensity as a function of λ. In this measurement, a new collimator system was employed to eliminate the contribution from the 'backing materials' behind the mercury/sapphire interface. Assuming an Ornstein–Zernike type permittivity correlation function, we have estimated the lateral correlation length and the interface width of the critical fluctuations to be several hundred nanometres and a few nanometres, respectively.

1. Introduction

The prewetting transition [1, 2] is a first-order phase transition between a thin and a thick wetting film on a substrate and has its own critical point. It has been about ten years since the first clear observation of the prewetting transition for ^{4}He on caesium [3], and there are several systems for which the phenomena have been observed. Mercury on sapphire is one such system, for which the prewetting critical point is located at $T_{cpw} = 1468\,^{\circ}$C and 159 MPa [4] whereas the bulk liquid–gas critical point is at $T_c = 1478\,^{\circ}$C and 167 MPa [5]. The nature of the prewetting transition and the average properties of the film in the subcritical phase have been widely studied experimentally for elemental liquids such as He [6] and Hg [7], binary liquids [8, 9] and liquid crystals [10]. However, very little is known on the supercritical one-phase region, where critical fluctuations or interfacial fluctuations are important.

[1] Author to whom any correspondence should be addressed.

For studying such fluctuations, an x-ray or neutron diffuse scattering experiment with grazing incidence is a powerful tool and its theoretical basis is well established [11]. However, the application of this technique to extreme conditions is quite difficult at the present stage. Hence alternative methods are required.

Recently, we found that thermal radiation measurement can also be used to study the fluctuations of the interface under high temperatures and pressures [12]. Indeed, the thermal radiation intensity from the mercury–sapphire interface shows an anomalous decrease in the prewetting supercritical region. This anomaly is a clear indication of the optical diffuse scattering caused by the critical fluctuations in the mercury wetting film.

The principle of thermal radiation measurement relies upon Kirchhoff's law, which relates the thermal radiation emitted from a surface of some body to its optical properties. The intensity $I_{\rm rad}$ of the radiation with wavelength λ from a unit area at angle θ to its normal is expressed as [13]

$$I_{\rm rad}(\lambda,\theta) = I_{\rm BB}(\lambda)A(\lambda,\theta)\cos(\theta). \tag{1}$$

Here, $I_{\rm BB}(\lambda)$ is the black-body radiation intensity and $A(\lambda,\theta)$ is the 'absorbing power' of the body. The fraction of light which is *not* absorbed by the body, $1 - A(\lambda,\theta)$, consists of the specular reflectivity term $R(\lambda,\theta)$ and the off-specular diffuse scattering term $\mathrm{d}\sigma/\mathrm{d}\Omega$ arising from the interfacial fluctuations. The scattering term should be integrated over the solid angle $\mathrm{d}\Omega$ into which the light is scattered. Thus the emissivity, which is defined as the radiation intensity normalized by the black-body radiation, can be written as

$$\begin{aligned} e(\lambda,\theta) &\equiv \frac{I_{\rm rad}(\lambda,\theta)}{I_{\rm BB}(\lambda)} \\ &= [1 - R(\lambda,\theta)]\cos\theta - \int \mathrm{d}\Omega\,\frac{1}{S}\,\frac{\mathrm{d}\sigma}{\mathrm{d}\Omega}, \end{aligned} \tag{2}$$

where S is the surface area. By using equation (2), we can obtain the diffuse scattering intensity from the emissivity data.

The application of this method to our system, however, suffers from some problems. Since the bulk fluid exists next to the wetting film, its density fluctuations could influence the emissivity spectrum as well, especially near the liquid–gas critical point. However, this problem may be bypassed in the present experiment, because the correlation length of the bulk density fluctuations is much shorter than the wavelength adopted in our work except for the close proximity of the critical point. In addition, one might think that the thermal radiation from the bulk fluid should cause another problem. However, when the fluid is transparent, no radiation is emitted in accordance with Kirchhoff's law, and when it is opaque on the other hand, all the radiations except for those from the mercury/sapphire interface are readily absorbed by the fluid itself. Thus the thermal radiation from the bulk fluid plays a minor role. A serious problem arises, however, when the thermal radiation emitted from 'backing materials' (BMs) such as the inner wall of the sample cell could be transmitted through the bulk sample and reach the detector. Thus we must carefully eliminate such background contributions from the emissivity spectrum. In the present work, we have measured the thermal radiation spectrum in the wavelength range $500 \lesssim \lambda < 1650$ nm and deduced the diffuse scattering intensity as a function of λ. In the measurements, a newly devised collimator system, which had not been used for making our previous measurements [12, 14], was employed to deduce the interfacial fluctuations properly by eliminating the background contributions.

The paper is arranged as follows. In section 2, we describe the experimental method. The results on the emissivity are presented in section 3. In section 4, we suggest a method for extracting the diffuse scattering due to the interfacial fluctuations from the measured emissivity,

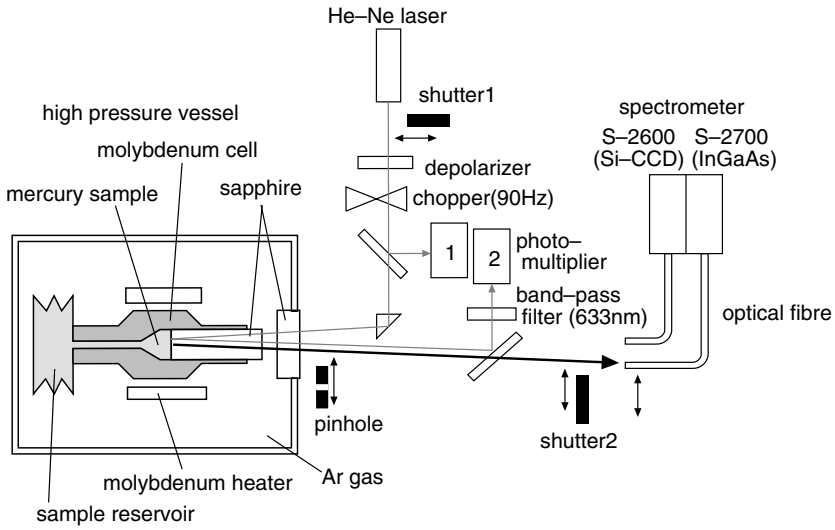

Figure 1. The experimental set-up for the simultaneous measurements of the thermal radiation intensity ($500 \lesssim \lambda < 1650$ nm) and the reflectivity ($\lambda = 633$ nm).

and discuss the two-dimensional critical fluctuations utilizing the estimated diffuse scattering spectrum. A summary is given in section 5.

2. Experiment

The mercury sample was encapsulated in a cylindrical molybdenum cell. A sapphire rod 6 mm in diameter and 95 mm in axial length, which served as an optical window, was inserted from one end of the cell, and the other end was connected to a sample reservoir. Near the central part of the cell, two molybdenum heaters were set and we could achieve high temperature states up to 1530 °C. The cell was put in a high pressure vessel, which was pressurized with argon gas, and we were able to achieve high pressure states up to 200 MPa. Details of the sample cell and the high pressure vessel have been given elsewhere [7, 15, 16].

The optical set-up for our measurements is shown in figure 1. We measured the reflectivity $R(\lambda = 633\ \text{nm}, \theta = 0)$ and the thermal radiation intensity $I_{\text{rad}}(500 \lesssim \lambda < 1650\ \text{nm}, \theta = 0)$ simultaneously. For the reflectivity measurement, we used a He–Ne laser as a light source and photomultipliers as detectors. In order to distinguish the reflected laser light from the thermal radiation, we used a band-pass filter and the lock-in detection technique. For the spectroscopic measurements of the thermal radiation intensity, two spectrometers, Soma Fastevert S-2600 and S-2700, were used as detectors: S-2600 is equipped with a Si CCD, whose sensitivity range is $300 < \lambda < 1000$ nm and S-2700 with an InGaAs photodiode array, which covers the wavelength range of $900 < \lambda < 1650$ nm. In our experimental conditions ($T \lesssim 1530$ °C), sufficient thermal radiation intensity was obtained for light with wavelengths above 500 nm.

The thermal radiation emitted from the hot part of the sample cell was collimated with a pinhole (1.5 mm in diameter) and introduced to each spectrometer through optical fibres (1 mm in diameter). Both the pinhole and the optical fibres were put on x-stages, whose positions were remotely controlled by a computer. Moving the end of the optical fibre relative to the pinhole, we scanned the sample part from which the radiation was emitted. Figure 2 shows a schematic illustration of the collimator system for the thermal radiation measurements. This collimator system was not employed in the previous works [12, 14].

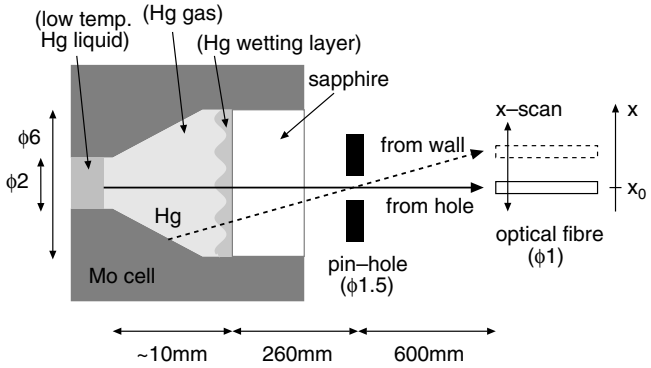

Figure 2. A schematic illustration of the collimator system for the thermal radiation measurements. When the mercury sample is gas, the capillary of the cell is filled with low temperature liquid mercury. Note that the molybdenum cavity wall of the cell makes an angle larger than 60° with the mercury/sapphire interface; this is arranged in order to avoid multiple reflection between them.

The detection system was calibrated by measuring the thermal radiation intensity as a function of wavelength at $d = 9$ g cm^{-3} and $T = 1405\,^{\circ}$C, where the relation $I_{\rm rad}(\lambda, \theta = 0) = I_{\rm BB}(\lambda)(1 - R(\lambda, \theta = 0))$ holds because the diffuse scattering term in equation (2) is neglected owing to the absence of wetting film at this density [7]. In addition, the bulk liquid mercury is optically thick, indicating that the radiation intensity can be calculated from the black-body radiation and the reflectivity of the mercury/sapphire interface. For this calibration, the reflectivity $R(\lambda, \theta = 0)$ data obtained by Hefner [17] and by Ohmasa *et al* [7] were used. The former data give a reliable λ dependence of reflectivity, and the latter give a reliable density dependence. The discrepancy between these two sets of data at $\lambda = 633$ nm and $d = 9$ g cm^{-3} is about 5%.

The optical measurements were carried out in a wide temperature and pressure range up to 1530 °C and 200 MPa. As shown in figure 3, the measurements were done with increasing temperature at nearly constant pressure (run number 1) and with decreasing pressures at constant temperatures (run numbers 2–7).

3. Results

3.1. Radiation intensity

Figure 4 shows representative resulting thermal radiation spectra against the wavelength. The data measured by the two spectrometers S-2600 (grey curve) and S-2700 (black curve) coincide well in the common wavelength range near 900 nm. The shape of the spectra is mainly determined by Planck's law (dashed curve) and also influenced by the wavelength dependence of the absorbing power of the sample. In figure 5 the thermal radiation intensities at various wavelengths are plotted as a function of the position x of the end of the optical fibre. When the sample is in the liquid state (figure 5(a)), the intensity changes little with the position, exhibiting a broad maximum around the centre, $x \sim x_0$. On the other hand, when the sample is dilute vapour (figure 5(b)), the intensity shows a substantial dip around the centre in the wavelength range 800 nm $\leqslant \lambda \leqslant$ 1500 nm, and the dip becomes deeper as the wavelength gets shorter. Since the emission from a thin film causes interference effects [18], one might regard the radiation intensity in figure 5(b) as the 'oscillation' due to such effects. However, the possibility is eliminated in this case because the period of the 'oscillation' is independent of the wavelength and the dip does not appear at 500 nm.

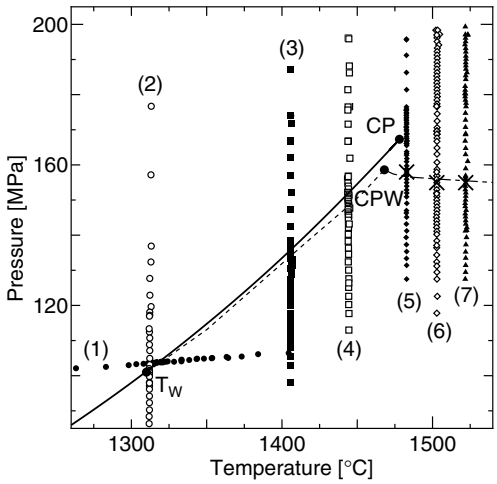

Figure 3. State points for the optical measurements. The numbers in the parentheses indicate the run numbers of the experiment. CP denotes the critical point of the bulk liquid–gas transition (solid curve), CPW the critical point of the prewetting transition (dashed curve) and T_W the wetting temperature. The locus (dot–dashed curve) of the maximum of 2D compressibility [4] and the state points (crosses) where the emissivity exhibits a minimum are also shown.

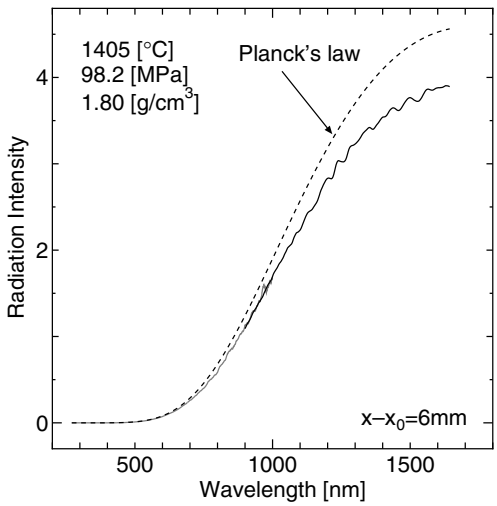

Figure 4. A thermal radiation spectrum from Hg vapour measured by the spectrometers S-2600 (grey line) and S-2700 (black curve). A black-body radiation spectrum (dashed curve) is also shown for comparison.

The origin of the dip can be explained by considering the contribution from the 'BM'. Here, the 'BM' means the material behind the mercury/sapphire interface, such as the molybdenum cavity wall and the capillary filled with liquid mercury (see figure 2). In the dilute gas state, the mercury sample is transparent in the long wavelength range. Hence, the radiation emitted from the BM also contributes to the measured radiation intensity. The dip is not observed at the wavelength of 500 nm, because the bulk mercury becomes opaque due to the increase in the absorption coefficient.

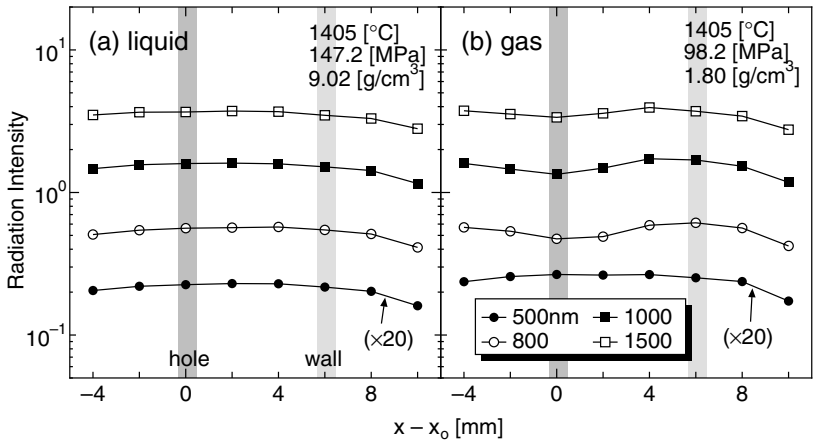

Figure 5. Thermal radiation intensity is shown as a function of the position x of the end of the optical fibre relative to the centre position x_0 for liquid Hg (a) and vapour (b). The intensity at the wavelength 500 nm is multiplied by 20 for clarity.

In the previous works [12, 14], the BM was assumed to be a black body with uniform temperature. However, the results of figure 5(b) indicate that this assumption is not accurate enough. For example, the absorbing power of the molybdenum cavity wall is smaller than unity and the temperature of the liquid mercury filling the capillary is slightly lower than that at the mercury/sapphire interface. Both of these effects tend to reduce the radiation intensity, but the latter effect is more efficient than the former, and this is why the intensity of the radiation emitted from the capillary (observed at $x - x_0 \sim 0$ mm) is smaller than that from the molybdenum wall ($x - x_0 \sim 6$ mm). Hereafter, we denote the data observed at $x - x_0 = 6$ mm by 'wall' and those at $x - x_0 = 0$ mm by 'hole', corresponding to BMs from which the radiation is emitted. We will discuss the effect of the BM in more detail in sections 4.1 and 4.3.

3.2. Pressure dependence of emissivity

In this subsection and the next one, we present the emissivity results for 'wall' as the BM, and the effects of different BMs will be given in section 3.4.

Figure 6 shows the results on reflectivity and emissivity at 1405 °C ($<T_{\mathrm{cpw}}$, run No 3 in figure 3) and 1502 °C ($>T_{\mathrm{c}} > T_{\mathrm{cpw}}$, run No 6 in figure 3). At 1405 °C the mercury sample is a liquid with high reflectivity at pressures above 136 MPa (figure 6(a)). When the pressure is decreased, the reflectivity shows a discontinuous decrease at 136 MPa, corresponding to the liquid–gas transition ('LG' in the figure), and it exhibits another drop at 134 MPa, corresponding to the prewetting transition ('PW' in the figure), where the thickness of the mercury wetting film on sapphire changes from thick to thin. In contrast to the reflectivity, the emissivity has a smaller value in the liquid state and a larger value in the gaseous state (figure 6(b)). This can be explained qualitatively via the relation $e_{\mathrm{obs}} = 1 - R_{\mathrm{Hg,sap}}$, where $R_{\mathrm{Hg,sap}}$ is the reflectivity at the mercury/sapphire interface.

When the temperature is higher than both T_{cpw} and T_{c}, the reflectivity (figure 6(c)) changes continuously over the whole pressure range. The reflectivity shows a minimum around 167 MPa, where the refractive index of mercury is equal to that of sapphire [7]. On the other hand, the emissivity (figure 6(d)) shows a distinct dip with a minimum around 150–160 MPa, where only a small kink is observed in the reflectivity. These observations

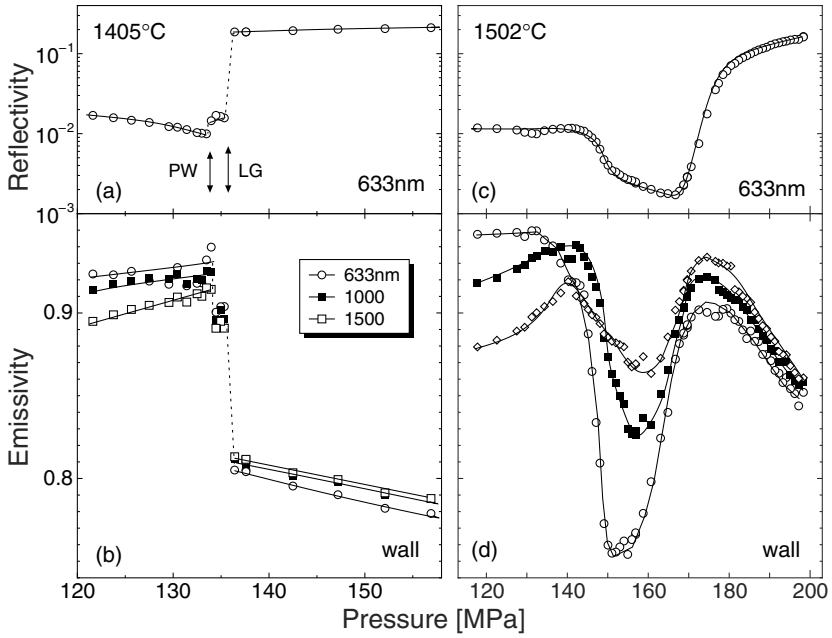

Figure 6. Representative results for the reflectivity and emissivity at 1405 °C ($<T_{\mathrm{cpw}}$) and 1502 °C ($>T_{\mathrm{c}} > T_{\mathrm{cpw}}$) at the wavelength of 633 nm (open circles), 1000 nm (closed squares) and 1500 nm (open squares). 'LG' indicates the liquid–gas transition and 'PW' the prewetting transition.

coincide completely with the previous results [12, 14]. The dip cannot be explained by the reflectivity term $1 - R_{\mathrm{Hg,sap}}$, and thus the scattering term has to be taken into account as given in equation (2). The dip becomes deeper as the wavelength becomes shorter, indicating that the scattering intensity increases with decreasing λ.

The state points where the emissivity exhibits a minimum are plotted with crosses in figure 3. These points fall on a curve (dot–dashed curve) in the figure. It should be noted that this curve agrees well with the line where anomalies were observed in early reflectivity measurements and interpreted as a phenomenon related to the maximum of the two-dimensional compressibility [4]. The prewetting transition has been discussed as a two-dimensional type of liquid–gas transition [19–21] and the increase of the two-dimensional compressibility near its critical point should appear in the strong scattering of light similarly to the critical opalescence of the bulk fluid. Hence, it is natural to assign the strong scattering observed along this line to the critical fluctuations of the prewetting transition [12].

3.3. Density dependence of emissivity

It is known that the most relevant parameter determining the physical properties of the bulk fluid mercury is the density [5]. In figure 7, the observed emissivity data at (a) 633 nm, (b) 800 nm and (c) 1500 nm are plotted against the density of bulk mercury. The different symbols indicate the run numbers shown in figure 3. In figure 7(a), the solid curve represents $1 - R^{\mathrm{bulk}}_{\mathrm{Hg,sap}}(633\ \mathrm{nm}, \theta = 0)$, where $R^{\mathrm{bulk}}_{\mathrm{Hg,sap}}(633\ \mathrm{nm}, \theta = 0)$ is the reflectivity at the mercury/sapphire interface without wetting film, calculated from the density dependence of the refractive index of bulk fluid mercury [7]. At densities higher than 7 g cm^{-3}, the measured emissivity depends little on temperature and coincides well with the solid curve. The same is

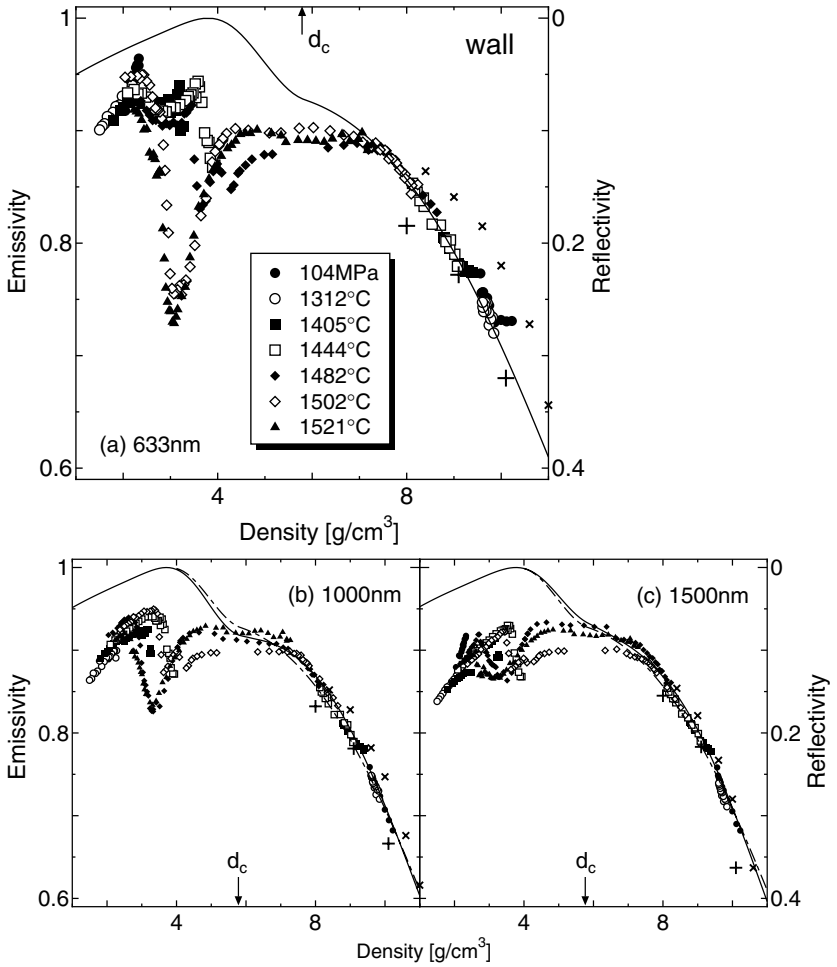

Figure 7. Emissivity is plotted at the wavelengths of (a) 633 nm, (b) 1000 nm and (c) 1500 nm against the density of bulk mercury. The different symbols indicate the run numbers shown in figure 3. The solid curves represent $1 - R^{\mathrm{bulk}}_{\mathrm{Hg,sap}}(\lambda, \theta = 0)$, where $R^{\mathrm{bulk}}_{\mathrm{Hg,sap}}(\lambda, \theta = 0)$ are the reflectivity at the mercury/sapphire interface, calculated from the refractive index of bulk fluid mercury (see [7] and section 4.2). For comparison $1 - R^{\mathrm{bulk}}_{\mathrm{Hg,sap}}(633\ \mathrm{nm}, \theta = 0)$ are shown by the dot–dashed curves in (b) and (c). Plus signs and crosses indicate $1 - R_{\mathrm{Hg,sap}}(\lambda, \theta = 0)$, where the reflectivities are due to Hefner [17] and Ikezi [22], respectively. d_c represents the critical density of mercury (5.8 g cm^{-3}).

also true for the wavelengths of 1000 nm (figure 7(b)) and 1500 nm (figure 7(c)), though the reflectivity depends on the wavelength as discussed in detail in section 4.2. These results prove the validity of the relation $e_{\mathrm{obs}} = 1 - R_{\mathrm{Hg,sap}}(\lambda, \theta = 0)$, and the absence of the wetting film in this density range. It should be noted that the density of the thick wetting film is estimated to be about 7 g cm^{-3} and that of the thin film is somewhat smaller [7]. When the density is decreased below 7 g cm^{-3}, the emissivity deviates downward from the solid curve, and the data above T_{cpw} (closed triangles, closed and open diamonds) show large dips around 3.0–3.5 g cm^{-3} due to the diffuse scattering. The dip becomes less pronounced as the wavelength gets longer in qualitative accordance with a common rule that the scattering is stronger for shorter wavelengths. At densities lower than about 2.6 g cm^{-3}, the emissivity becomes less

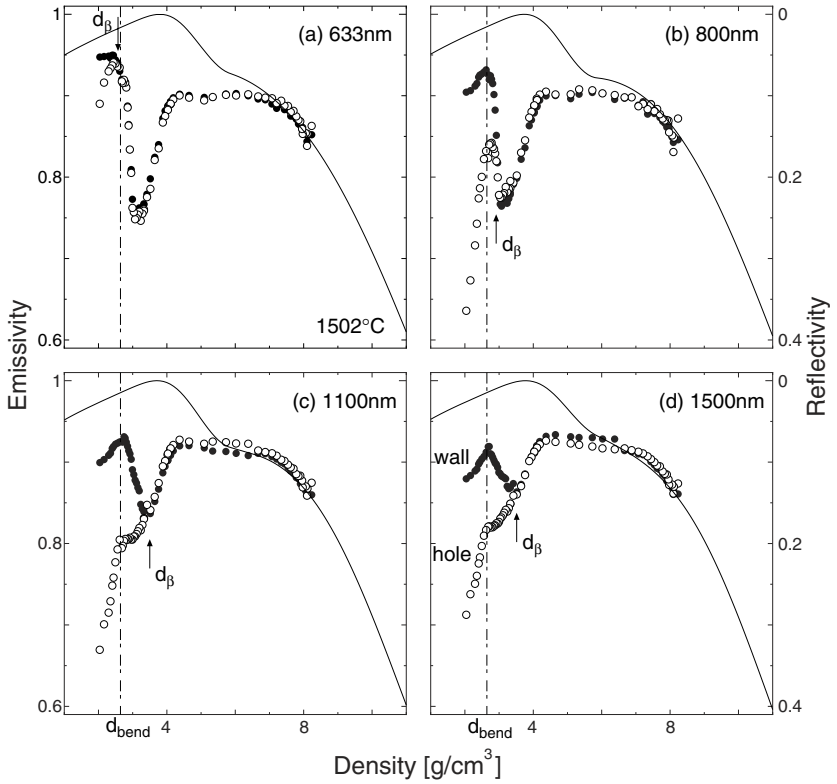

Figure 8. The density dependence of the emissivity at 1502 °C for 'hole' (open circle) and 'wall' (closed circle) as the BM at the wavelengths of (a) 633 nm, (b) 800 nm, (c) 1100 nm and (d) 1500 nm. The solid curves represent $1 - R^{\mathrm{bulk}}_{\mathrm{Hg,sap}}(\lambda, \theta = 0)$ for the bulk fluid mercury, as in figure 7 (see [7] and section 4.2). d_{bend} and d_β are the densities where the emissivity isotherms bend sharply and the difference of the two emissivity isotherms of different BMs appears, respectively.

temperature dependent and falls on a line that does not coincide with the solid curve. This discrepancy should be due to the effect of the BM, because in this low density region, the mercury sample becomes optically thin as the absorption coefficient of mercury decreases with decreasing density and the effect of the BM becomes important. We will discuss the effect of the BM in the later section 4.3.

3.4. Effect of backing material

Figure 8 shows the emissivity data observed at 1502 °C for the 'hole' (open circle) and 'wall' (closed circle) as the BM. The former corresponds to $x - x_0 = 0$ mm and the latter to $x - x_0 = 6$ mm in figure 5(b). The two emissivity curves coincide with each other over a wide density range. However, below some characteristic density, which we will refer to as the 'bifurcation' density d_β, there appears a marked difference between the two curves. It should be noted that d_β shifts to higher densities with increasing wavelength, as shown in figure 9. d_β can be interpreted as the density at which the bulk mercury sample changes from opaque to transparent and, as a result, the radiation from BMs begins to be transmitted through the sample. To prove this, we have estimated a threshold density d_θ in such a way that the optical thickness $1/\alpha$, where α represents the absorption coefficient of the bulk mercury, is equal to

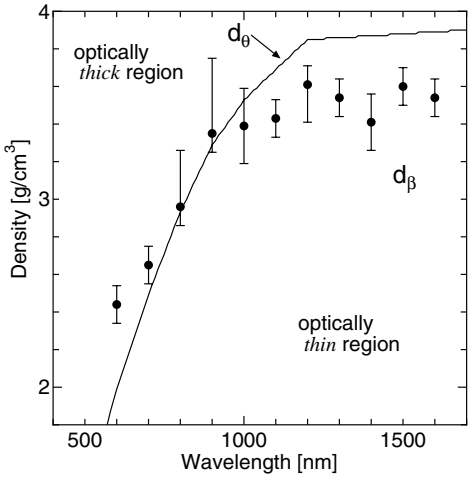

Figure 9. The 'bifurcation' density d_β (closed circles with error bars) deduced from the present emissivity data and the threshold density d_θ estimated from the absorption coefficient [23] are shown as a function of wavelength.

the sample thickness L at that density. In this estimation, we have used α obtained by Yao *et al* [23], and extrapolated it to the lower absorption or lower density region. The solid curve in figure 9 represents d_θ, which nearly coincides with d_β over a wide wavelength range.

Although the emissivity increases for the 'wall' and decreases for the 'hole' with decreasing density below d_β, all the emissivity curves exhibit a sharp bend, irrespective of the BM, at a density $d_{\rm bend} \sim 2.6$ g cm^{-3} (see figure 8). Since $d_{\rm bend}$ does not depend on the wavelength, the bend cannot be related to the optical absorption of the bulk mercury and should be attributed to some changes in the mercury/sapphire interfacial properties. Furthermore, because the reflectivity do not show an abrupt change at $d_{\rm bend}$ (figure 6 and [7, 15]), the bend cannot be connected with the average properties of the wetting film. Thus, it is reasonable to think that the scattering due to the interfacial fluctuations in the mercury wetting film on sapphire is strong at densities higher than $d_{\rm bend}$ whereas it is less important at lower densities. Near $d_{\rm bend}$, small fluctuations may induce larger fluctuations because the permittivity of fluid mercury is highly state dependent, unlike those of ordinary insulating fluids.

The emissivity spectrum observed at 1502 °C and 117.8 MPa, where the density of bulk mercury is 2.04 g cm^{-3}, is displayed for the 'wall' (figure 10(a)) and the 'hole' (figure 10 (b)) by the bold solid curves. Except for the wavelength range below 600 nm, these two spectra exhibit rather different behaviours. Especially above 800 nm, the emissivity *decreases* with increasing λ for the 'wall', while it *increases* for the 'hole'. A quantitative analysis of the emissivity spectra will be given in section 4.3.

4. Discussion

We first devise a modified formula to describe the emission intensity in section 4.1. Then the optical properties of *bulk* mercury and BMs are estimated in sections 4.2 and 4.3, and by using such information the scattering intensity is extracted from the emissivity spectrum in section 4.4. Finally, we discuss the prewetting critical fluctuations from the scattering intensity in 4.5.

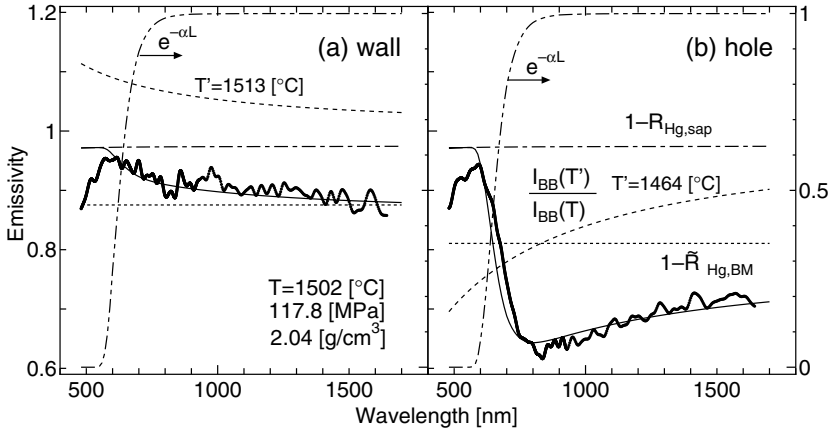

Figure 10. Emissivity spectra for the 'wall' (a) and 'hole' (b). The bold solid curves illustrate the experimental spectra observed at 1502 °C and 117.8 MPa, where the density of bulk Hg is 2.04 g cm^{-3}. The thin solid curves indicate the emissivity calculated from equation (6). The quantities used in this calculation, $1-\tilde{R}_{\mathrm{Hg,BM}}$, $1-R_{\mathrm{sap,Hg}}$, $I_{\mathrm{BB}}(T')/I_{\mathrm{BB}}(T)$ and $\mathrm{e}^{-\alpha L}$, are indicated by the dotted, dot–dashed, dashed and dot–dot–dashed curves, respectively.

4.1. A modified formula for the emission intensity

As described in sections 3.1 and 3.4, the thermal radiation intensity deviates from the equation (2) in the dilute gas region. In order to explain the radiation intensity in this region, we need to take account of the optical absorption of bulk fluid mercury, the absorbing power of the BM and the temperature inhomogeneity in the sample cell. Figure 11 shows a model of the sample part of the cell including the BMs used for devising a modified formula to describe the emission intensity. The thickness and the absorption coefficient of the bulk mercury sample are represented by L and α, respectively. The thickness L is about 10 mm. The temperature of the mercury sample, T, and that of the BM, T', are not necessarily equal in this model. $\tilde{R}_{\mathrm{Hg,sap}}$ and $\tilde{R}_{\mathrm{Hg,BM}}$ are 'total reflectivities' at the mercury/sapphire and the mercury/BM interfaces, respectively. Here, the 'total reflectivity' $\tilde{R}_{\mathrm{a,b}}$ at the a-phase/b-phase interface is defined as the sum of the specular reflectivity $R_{\mathrm{a,b}}$ and the off-specular diffuse scattering intensity:

$$\tilde{R}_{\mathrm{a,b}} = R_{\mathrm{a,b}} + \int \mathrm{d}\Omega \, \frac{1}{S} \, \frac{\mathrm{d}\sigma}{\mathrm{d}\Omega}. \tag{3}$$

In this model, the following assumptions are made:

(i) The sapphire window does not emit radiation because it is transparent.
(ii) The wetting film on the sapphire substrate is optically thin enough, and both the absorption by the film and the radiation from the film are negligible. Indeed, the thickness l of the wetting film is estimated at $l \sim 10$ nm [7], which is much smaller than the optical thickness $1/\alpha$. Thus the properties of the wetting film are characterized just by the total reflectivity $\tilde{R}_{\mathrm{Hg,sap}}$. The interference effect within the film is included in $R_{\mathrm{Hg/sap}}$.
(iii) The *bulk* mercury can be treated as a homogeneous medium, because the correlation length of the bulk density fluctuations is much shorter [24, 25] than the wavelength adopted in our work except for the close proximity of the critical point.
(iv) The total reflectivity at the mercury/BM interface, $\tilde{R}_{\mathrm{Hg,BM}}$, changes moderately with temperature and pressure.
(v) The multiple-reflection effect between the Hg/BM and Hg/sapphire interfaces is neglected.

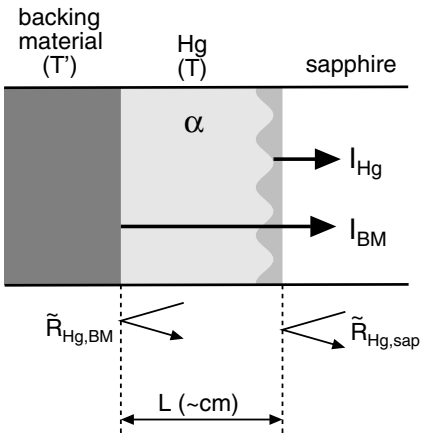

Figure 11. A model of the sample part of the cell used for the calculation of the thermal radiation intensity. Note that the distance between the BM and the sapphire is macroscopic (∼cm).

The measured total radiation intensity should contain two terms: the radiation from the mercury, $I_{\rm Hg}$, and that from the BM, $I_{\rm BM}$. They are expressed as

$$I_{\rm Hg} = I_{\rm BB}(T)(1 - \tilde{R}_{\rm Hg,sap})(1 - {\rm e}^{-\alpha L}), \tag{4}$$

$$I_{\rm BM} = I_{\rm BB}(T')(1 - \tilde{R}_{\rm Hg,BM}){\rm e}^{-\alpha L}(1 - \tilde{R}_{\rm Hg,sap}). \tag{5}$$

Here $I_{\rm BB}(T)$ is the radiation intensity from a black body kept at temperature T (Planck's law). When the mercury is not optically thick, the intensity from the mercury is reduced by a factor of $1 - {\rm e}^{-\alpha L}$ which is the power of absorption in the bulk fluid mercury. The radiation intensity from the BM is determined by the three factors. The first factor is the intensity of the radiation emitted from the mercury/BM interface, $I_{\rm BB}(T')(1 - \tilde{R}_{\rm Hg,BM})$. The second and third factors are the transmission coefficients of the bulk mercury and the mercury/sapphire interface, ${\rm e}^{-\alpha L}$, and $1 - \tilde{R}_{\rm Hg,sap}$, respectively.

From the equations (4) and (5), the total emissivity observed by the detectors can be obtained from

$$e_{\rm obs} = \frac{I_{\rm Hg} + I_{\rm BM}}{I_{\rm BB}(T)}$$

$$= (1 - \tilde{R}_{\rm Hg,sap})\left[1 - {\rm e}^{-\alpha L} + \frac{I_{\rm BB}(T')}{I_{\rm BB}(T)}(1 - \tilde{R}_{\rm Hg,BM}){\rm e}^{-\alpha L}\right] \tag{6}$$

$$= \begin{cases} 1 - \tilde{R}_{\rm Hg,sap} & (\alpha L \gg 1) \quad (7a) \\ (1 - \tilde{R}_{\rm Hg,sap})(1 - \tilde{R}_{\rm Hg,BM})\dfrac{I_{\rm BB}(T')}{I_{\rm BB}(T)} & (\alpha L \ll 1). \quad (7b) \end{cases}$$

When the sample is opaque ($\alpha L \gg 1$), $e_{\rm obs}$ is given by equation (7*a*), and depends only on the properties of the mercury/sapphire interface. In this limit, $e_{\rm obs}$ coincides with equation (2) with $\theta = 0$. When the sample is transparent ($\alpha L \ll 1$), $e_{\rm obs}$ is represented by equation (7*b*), which depends not only on the properties of the mercury/sapphire interface but also on those of the BM.

In the previous works [12, 14], we assumed that the BM is a black body ($\tilde{R}_{\rm Hg,BM} = 0$) and the temperature in the sample cell is uniform ($T = T'$). In such a special case, $e_{\rm obs}$ in equation (6) is simply reduced to $1 - \tilde{R}_{\rm Hg,sap}$ irrespective of αL.

4.2. Optical properties of bulk mercury

In this subsection, we have to estimate the density and the wavelength dependence of the complex refractive index $\tilde{n} = n + \mathrm{i}k$ of *bulk* fluid mercury from the observed emissivity data, because the optical constants [17, 22] derived from the reflectivity measurement do not show smooth density variations.

In the previous work [7], the density dependence of n and k for the wavelength $\lambda = 633$ nm was calculated from the optical reflectivity data, which was measured under normal reflection and 45° reflection conditions over a wide density range. In this calculation, n and k were assumed to be smooth functions of density, $n(d)$ and $k(d)$, that satisfy the following requirements:

(i) In the low density region $d < d_n = 2.0$ g cm^{-3}, $n(d)$ should have the form of a Lorentz–Lorenz formula $(1 + 2Cd)/(1 - Cd)$ with a parameter C which is proportional to the polarizability of an isolated atom. As the density increases, $n(d)$ deviates upward from this formula.

(ii) In the low density region $d < d_k = 5.0$ g cm^{-3}, $k(d)$ should be regarded as zero because the optical absorption coefficient in this region is very small.

(iii) Under ambient conditions with the density $d = 13.6$ g cm^{-3}, $n(d)$ and $k(d)$ should coincide with the values of [26].

(iv) The above mentioned two extrema should be connected to each other by smooth curves in the intermediate density region ($d_n < d < 13.6$ g cm^{-3} for n and $d_k < d < 13.6$ g cm^{-3} for k).

Thus, we employed the following trial functions:

$$n(d) = \begin{cases} \sqrt{\dfrac{1+2Cd}{1-Cd}} + g(d) & (0 \leqslant d \leqslant d_n = 2 \text{ g cm}^{-3}), \\ n_0 + n_1(d - d_n) + n_2(d - d_n)^2 + g(d) & (d_n < d \leqslant 13.6 \text{ g cm}^{-3}), \end{cases} \tag{8}$$

$$k(d) = \begin{cases} 0 & (0 \leqslant d \leqslant d_k), \\ k_1(d - d_k) + k_2(d - d_k)^2 & (d_k < d \leqslant 13.6 \text{ g cm}^{-3}), \end{cases} \tag{9}$$

where

$$g(d) = \begin{cases} g_0 \exp[-((d - d_0)/\sigma_1)^2] & (d \leqslant d_0), \\ g_0 \exp[-((d - d_0)/\sigma_2)^2] & (d \geqslant d_0) \end{cases} \tag{10}$$

is an asymmetric Gaussian function, which was introduced to reproduce the plateau of the reflectivity around $d = d_0 = 5.85$ g cm^{-3}. n_0 and n_1 were determined from the condition that $n(d)$ and its first derivative are continuous at d_n. The density dependence of the observed reflectivity at 633 nm is well reproduced by adjusting the six free parameters C, g_0, d_0, σ_1, σ_2 and k_1.

In the present work, we try to extend this functional form to the refractive index at various wavelengths. First, to avoid too much complexity, we fix some parameters at the values obtained previously at $\lambda = 633$ nm. At the lowest densities, $d < d_n = 2.0$ g cm^{-3}, the 6s–6p energy gap is so large that C may be treated as constant in the present wavelength range. Consequently, n_0 and n_1 can be also fixed. Since d_0 is very close to the critical density, which serves as a good scaling parameter, d_0 together with σ_1 and σ_2 may be fixed too. Next, the other parameters n_2, g_0, d_k, k_1 and k_2 in equations (8)–(10) are expressed as cubic polynomial functions of λ:

$$y(\lambda) = \sum_{i=0}^{3} y_i \lambda^i \qquad (y = n_2, g_0, d_k, k_1 \text{ and } k_2; \lambda \text{ in units of } \mu\text{m}). \tag{11}$$

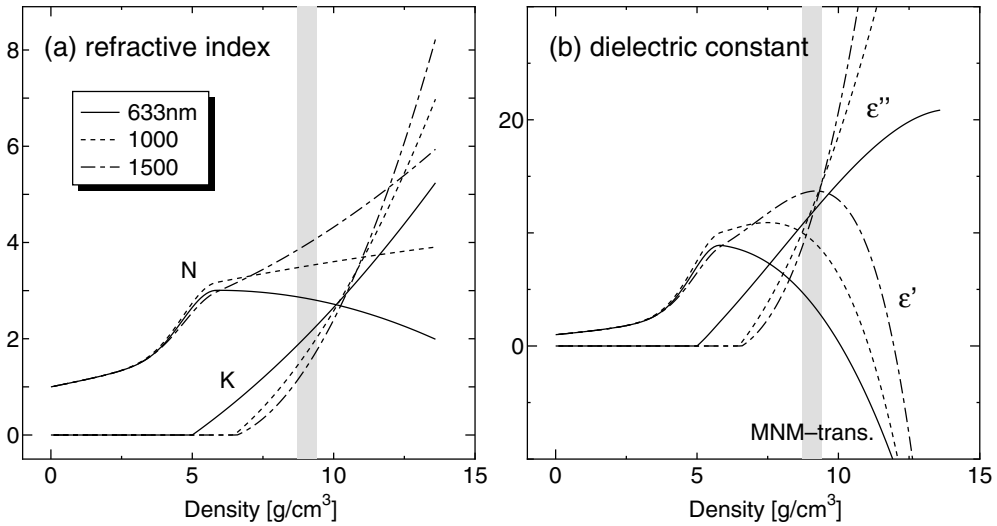

Figure 12. The complex refractive index $\tilde{n} = n + \mathrm{i}k$ (a) and the dielectric constant $\tilde{\epsilon} = \epsilon' + \mathrm{i}\epsilon''$ (b) of bulk fluid mercury estimated from the emissivity data. The solid, dashed and dot–dashed curves represent the optical constants at 633, 1000 and 1500 nm, respectively. The shaded area indicates the metal–nonmetal transition region.

Except for d_k, which can be deduced directly from the optical absorption spectra in [23], these parameters are to be determined by fitting. Therefore, 16 coefficients n_{2i}, k_{1i}, k_{2i} and g_{0i} ($i = 0, 1, 2, 3$) are adjusted to minimize the discrepancy factor D defined by

$$D = \sum_{\text{data}} \sum_{\lambda} [e^{\text{obs}} - (1 - R^{\text{calc}}_{\text{Hg,sap}})]^2 \tag{12}$$

where e^{obs} is the measured emissivity and $R^{\text{calc}}_{\text{Hg,sap}}$ represents the reflectivity at the mercury/sapphire interface calculated from the refractive index of bulk mercury. We used all the emissivity data e^{obs} in the density range $d > 7.0$ g cm^{-3}, where no wetting film exists. Further details of the analysis are described elsewhere [16]. The resultant values from these procedures are given in table 1. Figure 12(a) shows the complex refractive index $\tilde{n} = n + \mathrm{i}k$ of bulk fluid mercury. The emissivity $1 - R_{\text{Hg,sap}}$ calculated from the bulk optical constants is indicated in figures 7(b) and (c) by solid curves, which reproduce well the observed emissivity above 7 g cm^{-3}.

Figure 12(b) shows the complex dielectric constant $\tilde{\epsilon} = \epsilon' + \mathrm{i}\epsilon'' = \tilde{n}^2$ of bulk fluid mercury. The real part of the dielectric constant ϵ' shows a maximum and its peak position shifts to larger density as the wavelength gets longer. The peak position reaches the metal–nonmetal transition density (9 g cm^{-3}) at the long wavelength limit. This feature is consistent with a theoretical prediction of a dielectric anomaly near the metal–nonmetal transition [27].

4.3. Optical properties of backing material

As shown in figure 10, the emissivity spectrum at low densities depends largely on the BM. In this subsection, we demonstrate that such BM effects can be explained quantitatively by equation (6).

At 1502 °C and 117.8 MPa, where the density of bulk mercury is 2.04 g cm^{-3}, the wetting film is quite thin and the interfacial fluctuations are negligible. Thus the total reflectivity $\tilde{R}_{\text{Hg,sap}}$ appearing in equation (6) may be replaced by the reflectivity at the interface between

Table 1. Parameters for the density and the wavelength dependence of the bulk refractive indices $n(d, \lambda)$ and $k(d, \lambda)$ (see equations (8)–(11)). The parameters C, n_0, n_1, d_0, σ_1 and σ_2 in the upper table are fixed to the values estimated from the reflectivity data at 633 nm [7]. The coefficients in the lower table describe the wavelength dependence (see equation (11)) of n and k estimated from the present emissivity measurement (n_2, g_0, k_1 and k_2) and the optical adsorption data in [23] (d_k).

C ($\mathrm{cm^3\ g^{-1}}$)	n_0	n_1 ($\mathrm{cm^3\ g^{-1}}$)	d_0 ($\mathrm{g\ cm^{-3}}$)	σ_1 ($\mathrm{g\ cm^{-3}}$)	σ_2 ($\mathrm{g\ cm^{-3}}$)
0.0794	1.66	0.135	5.85	1.68	254

i	0	1	2	3
n_2 ($\mathrm{cm^6\ g^{-2}}$)	−0.0317	0.005 69	0.0343	−0.0111
g_0	0.418	3.25	−2.85	0.614
k_1 ($\mathrm{cm^3\ g^{-1}}$)	0.181	0.311	0.309	−0.321
k_2 ($\mathrm{cm^6\ g^{-2}}$)	−0.0521	0.126	−0.0244	0.0150
d_k ($\mathrm{g\ cm^{-3}}$)	−3.00	20.2	−13.9	3.14

the bulk mercury vapour and the sapphire substrate, which can be estimated from the optical constants determined in the last section. The result is illustrated by the dot–dashed curves in figure 10. The absorption coefficient α is taken from [23], and the sample thicknesses L is determined geometrically to be 5 mm for the 'wall' and 10 mm for the 'hole'. It is noted that $\mathrm{e}^{-\alpha L}$ varies rapidly with λ, as indicated by the dot–dot–dashed curves. To proceed the calculation further, we assume that the reflectivity $\tilde{R}_{\mathrm{Hg,BM}}$ at the mercury/BM interface does not depend on the wavelength. $\tilde{R}_{\mathrm{Hg,BM}}$ determine the asymptotic values of emissivity at the long wavelength limit where $\mathrm{e}^{-\alpha L}$ approaches unity and $I_{\mathrm{BB}}/I_{\mathrm{BB}'}$ approaches T/T', as shown by the dotted curves. The most important factor that characterizes the asymptotic behaviour of the emissivity is $I_{\mathrm{BB}}(T')/I_{\mathrm{BB}}(T)$, which increases with λ for $T > T'$ and decreases for $T < T'$, as shown by the dashed curves.

The calculated emissivity spectra are denoted by the thin solid curves, which reproduce well the experimental curves except for the short wavelength region. The temperature for 'wall' is higher than that of the sample by $11 \pm 5\,^{\circ}\mathrm{C}$. This result is consistent with the experimental situation that the molybdenum cell was located more closely to the heater than the mercury sample, as shown in figure 1. In fact the temperature at the outer wall of the molybdenum cell was higher than that of the sample by $16 \pm 2\,^{\circ}\mathrm{C}$. On the other hand, the temperature of 'hole' is lower than that of the sample by $38 \pm 10\,^{\circ}\mathrm{C}$. This is because the vapour/liquid interface in the 'hole' was situated apart from the hottest part of cell which is filled with the vapour (see figure 2). The reflectivity at the mercury/BM interface $\tilde{R}_{\mathrm{Hg,BM}}$ is estimated to be 0.12 ± 0.04 for the 'wall' and 0.18 ± 0.04 for the 'hole'. The former value is rather smaller than the typical reflectivity $R > 0.5$ at the metal/gas interface, which can be explained by the roughness of the wall being very large because the molybdenum wall was not polished or because the mercury wetting film is formed on it.

The same calculations have been performed for higher densities, and the agreement between the calculated and experimental emissivities is found to be satisfactory as long as the density is smaller than d_{bend}. Above this density, however, the scattering effects play a major role.

4.4. Estimation of the scattering intensity

In this subsection, we deduce the scattering intensity at the mercury/sapphire interface from the measured emissivity. For this purpose, we first estimate the emissivity intensity that

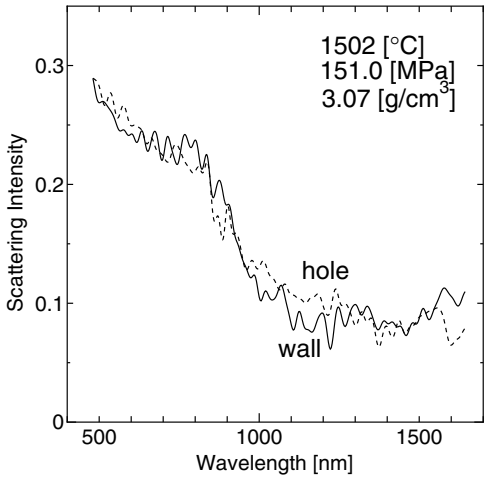

Figure 13. Scattering intensities at 1502 °C and 151.0 MPa calculated for the 'wall' (solid curve) and 'hole' (dashed curve).

would be expected if there were no scattering. We refer to this hypothetical quantity as the specular reflectivity, e_{specular}, because only the specular reflectivity term is taken to $\tilde{R}_{\text{Hg,sap}}$ in equation (6):

$$e_{\text{specular}} \equiv (1 - R_{\text{Hg,sap}})\left[1 - \mathrm{e}^{-\alpha L} + \frac{I_{\text{BB}}(T')}{I_{\text{BB}}(T)}(1 - \tilde{R}_{\text{Hg,BM}})\mathrm{e}^{-\alpha L}\right]. \tag{13}$$

As shown in figure 6, the difference between the reflectivities with and without the wetting film is of the order of 10^{-2}, which is negligible compared to the scattering term ($\sim 10^{-1}$). Therefore, we can replace the reflectivity at the mercury/sapphire interface, $R_{\text{Hg,sap}}$, in (13) by the reflectivity against the *bulk* mercury without the wetting film, $R^{\text{bulk}}_{\text{Hg,sap}}$. The latter is calculated from the optical properties of the bulk mercury estimated in section 4.2. α is taken from [23]. T' and $\tilde{R}_{\text{Hg,BM}}$ are calculated by extrapolating the values estimated in section 4.3 to the higher density region.

Then the scattering intensity is calculated from

$$\int \mathrm{d}\Omega \, \frac{1}{S} \, \frac{\mathrm{d}\sigma}{\mathrm{d}\Omega} = (1 - R_{\text{Hg,sap}})\left(1 - \frac{e_{\text{obs}}}{e_{\text{specular}}}\right), \tag{14}$$

Here we make use of equations (6) and (13). The representative results for the estimated scattering intensity at 1502 °C and 151.0 MPa are shown in figure 13. The solid and dashed curves represent the scattering intensities calculated for the 'wall' and 'hole' data, respectively. The two scattering intensities coincide well, indicating that the influence of the BM is successfully removed by this procedure. We have confirmed the consistency of the two scattering intensities at various pressures and temperatures. For this reason, only the scattering intensity estimated from the data for 'wall' will be presented hereafter.

The pressure dependence of the scattering intensity is shown in figure 14. The scattering intensity exhibits a maximum around 155 MPa. As the wavelength becomes shorter, the peak grows and its position shifts slightly to lower pressures. Figure 15 displays the scattering intensity isotherms at three different temperatures in the prewetting supercritical region ($T > T_{\text{cpw}}$). The wavelength is (a) 633 nm and (b) 1500 nm. When the temperature decreases toward the prewetting critical temperature T_{cpw}, the peak width diminishes for the both wavelengths. The peak height remains nearly constant at 1500 nm and, unexpectedly, it

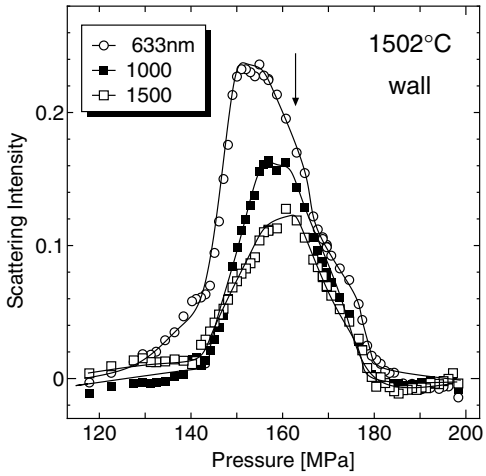

Figure 14. Pressure dependences of the scattering intensity at 1502 °C for 633 nm (open circles), 1000 nm (solid squares) and 1500 nm (open squares). The arrow indicates the state point where the scattering spectrum is presented in figure 16.

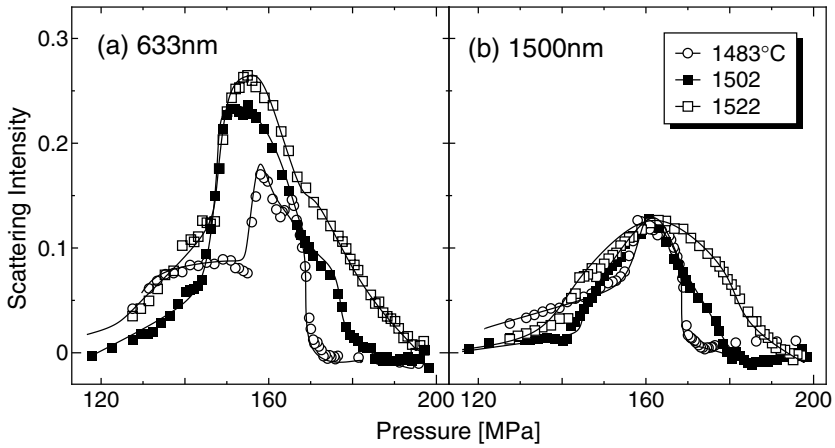

Figure 15. Scattering intensity isotherms at 1483 °C (open circles), 1502 °C (solid squares) and 1522 °C (open squares) in the prewetting supercritical region ($T > T_{cpw} = 1468$ °C). The wavelength is (a) 633 nm and (b) 1500 nm.

decreases at 633 nm. The reduction of peak height may be explained partially by the fact that, as the temperature decreases, the permittivity of the bulk gas phase increases toward that of the wetting film, leading to the reduction of the permittivity fluctuations (see equations (18)). Another possible explanation is that the interfacial fluctuations are suppressed by the strong surface potential from the sapphire substrate.

4.5. Prewetting critical fluctuations

Figure 16 shows representative results for the scattering intensity at 1502 °C and 163.1 MPa as a function of the wavelength. The state point is indicated by the arrow in figure 14. As expected, the scattering intensity decreases with the wavelength. However, the λ dependence

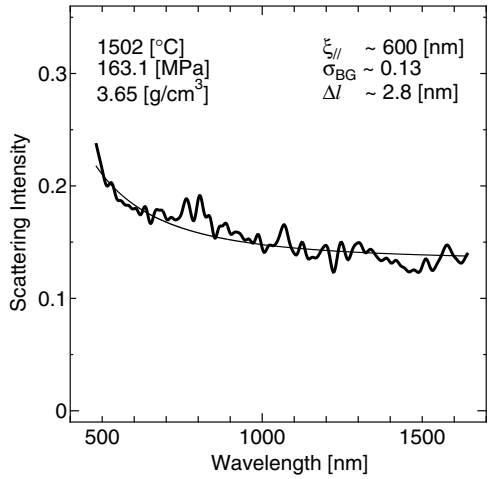

Figure 16. The wavelength dependence of the scattering intensity at 1502 °C and 163.1 MPa. The bold solid curve shows the estimated scattering intensity and the thin solid curve the result of fitting by equation (18). The state point corresponds to the arrow in figure 14.

of the scattering intensity is much weaker than the Rayleigh λ^{-4} law, and this λ dependence can be explained by taking into account the spatial correlation length of the fluctuation.

The cross section of the optical scattering caused by the interfacial fluctuations can be expressed in terms of the Fourier transform, $G(\vec{p}, z, z')$, of the two-point correlation function, $\langle\tilde{\epsilon}^*(\vec{r}, z)\tilde{\epsilon}(\vec{r}', z')\rangle$, of the permittivity fluctuation $\tilde{\epsilon}(\vec{r}, z)$ [11],

$$\frac{1}{S}\frac{\mathrm{d}\sigma}{\mathrm{d}\Omega} = \frac{\pi^2}{\lambda^4}\int\int \mathrm{d}z\,\mathrm{d}z'\,G(\vec{p}, z, z')F(\lambda, z, z') \tag{15}$$

$$G(\vec{p}, z, z') = \int\int \mathrm{d}^2\vec{r}'\,\langle\tilde{\epsilon}^*(\vec{r}, z)\tilde{\epsilon}(\vec{r}+\vec{r}', z')\rangle \mathrm{e}^{\mathrm{i}\vec{p}\cdot\vec{r}'} \tag{16}$$

where $\vec{r} = (x, y)$ and z are the coordinates parallel and normal to the surface, and $\vec{p}$ is the momentum transfer parallel to the surface. $F(\lambda, z, z')$ is a complicated function of the electric fields at z and z' [11]. In the present work, we assume that $F(\lambda, z, z') \simeq 1.0$, since $F(\lambda, z, z')$ varies slowly with λ, z and z' and its value is of the order of unity.

In order to estimate $G(\vec{p}, z, z')$, we make the following assumptions. First, we assume that the fluctuations are spatially restricted within the liquid/vapour interface region of the wetting film, namely, that $l - \Delta l/2 < z < l + \Delta l/2$, where l is the mean thickness of the layer. This assumption is valid when the fluctuation in the permittivity is mainly due to the fluctuation in the film thickness around its mean value l. Second, we assume that $G(\vec{p}, z, z')$ has a functional form of the Ornstein–Zernike type. This form is usually used to analyse the lateral density correlation function near the prewetting critical point via both theory [28] and simulation [29], and the Landau expression of the free energy for a thin film with a sharp-kink approximation directly gives the height–height correlation function of this form [30]. Then, $G(\vec{p}, z, z')$ can be written as

$$G(\vec{p}, z, z') = \begin{cases} \dfrac{\xi_\parallel^2|\Delta\epsilon|^2}{1+\xi_\parallel^2|\vec{p}|^2} & \text{for } l - \Delta l/2 < z, \quad z' < l + \Delta l/2, \\ 0 & \text{otherwise,} \end{cases} \tag{17}$$

where $\xi_\parallel$ is the correlation length in the lateral plane; $\Delta\epsilon$ is the strength of the permittivity

fluctuation, which is nearly equal to the difference in permittivity between the bulk gas phase and the wetting film. Hence, the scattering intensity is expressed as

$$\int \mathrm{d}\Omega \, \frac{1}{S} \frac{\mathrm{d}\sigma}{\mathrm{d}\Omega} = \frac{\pi^2}{\lambda^4} (\Delta l)^2 |\Delta\epsilon|^2 \int \mathrm{d}\Omega' \, \frac{\xi_\parallel^2}{1 + \xi_\parallel^2 |\vec{p}|^2} + \sigma_{\mathrm{BG}}. \tag{18}$$

Here we introduce a 'white' background term σ_{BG}, which does not depend on the wavelength. The background term may be caused by multiple-scattering effect.

When $\xi_\parallel$ is much smaller than λ, the first term of the equation (18) is proportional to λ^{-4}, because $|\vec{p}|$, which is of the order of $2\pi/\lambda$, is negligible. When $\xi_\parallel \gtrsim \lambda$, on the other hand, the λ dependence of this term deviates from the λ^{-4} law. Therefore, we can estimate the lateral correlation length $\xi_\parallel$ from the λ dependence of the scattering intensity.

We adjust three parameters $\xi_\parallel$, Δl and σ_{BG} to fit the estimated scattering intensity by using equation (18). The fitting result is shown in figure 16 for the scattering data at 1502 °C and 163.1 MPa, by the solid curve. The observed scattering intensity is well fitted by the parameters $\xi_\parallel \sim 600$ nm, $\Delta l \sim 2.8$ nm and $\sigma_{\mathrm{BG}} \sim 0.13$. The correlation length obtained, $\xi_\parallel$, is quite large compared to the thickness of the wetting film (∼10 nm [7]), and the interface width Δl is larger than the bulk correlation length ($\lesssim$1 nm [24]).

One might think that the estimated $\xi_\parallel$ is too large for the condition of not being in close proximity to the prewetting critical point, i.e. $(T - T_{\mathrm{cpw}})/T_{\mathrm{cpw}} \sim 0.02$. However, it is not surprising because the interface width depends logarithmically on the lateral correlation length [30, 31], predicting that a slight increase of Δl results in a substantial enhancement of $\xi_\parallel$.

It would be very interesting to elucidate how $\xi_\parallel$ and Δl vary on approaching the prewetting critical point. However, it is still difficult at this stage to estimate these quantities accurately enough to deduce reliable temperature and pressure dependences.

5. Summary

The thermal radiation intensity from the mercury/sapphire interface shows an anomalous decrease in the prewetting supercritical region. This anomaly is a clear indication of the optical diffuse scattering caused by the critical fluctuations in the mercury wetting film formed on the sapphire substrate. In the present work, we employed a new collimator system and measured the thermal radiation spectrum in the wavelength range $500 \lesssim \lambda < 1650$ nm. For the analysis, a modified model, which considers the contribution from the 'BM' behind the mercury/sapphire interface to the observed radiation intensity, was devised. We used this model and deduced the diffuse scattering intensity as a function of the wavelength. By assuming an Ornstein–Zernike type permittivity correlation function, we estimated the lateral correlation length and the interface width of the critical fluctuations to be several hundred nanometres and a few nanometres, respectively. The former value is much larger than the thickness of the wetting film (∼10 nm) and the latter is also larger than the bulk correlation length ($\lesssim$1 nm), which is qualitatively consistent with the theory. We also estimated the density and the wavelength dependence of the refractive index of bulk mercury from the emissivity.

Acknowledgments

We are grateful to Dr H Kohno and Messrs Y Hiejima, H Kajikawa and K Abe for collaboration on the experiment. We also thank Professor S Dietrich for valuable discussions. This work was partially supported by a grant-in-aid for Scientific Research (13740217, 14340106) from the Ministry of Education, Science, Sports and Culture, Japan.

References

[1] Cahn J W 1977 *J. Chem. Phys.* **66** 3667
[2] Ebner C and Saam W F 1977 *Phys. Rev. Lett.* **38** 1486
[3] Rutledge J E and Taborek P 1992 *Phys. Rev. Lett.* **69** 937
[4] Yao M and Hensel F 1996 *J. Phys.: Condens. Matter* **8** 9547
[5] Hensel F and Warren W W Jr 1999 *Fluid Metals* (Princeton, NJ: Princeton University Press) chapter 4
[6] Phillips J A, Ross D, Taborek P and Rutledge J E 1998 *Phys. Rev.* B **58** 3361
[7] Ohmasa Y, Kajihara Y and Yao M 2000 *Phys. Rev.* E **63** 051601
[8] Bonn D and Ross D 2001 *Rep. Prog. Phys.* **64** 1085
[9] Staroske S, Freyland W and Nattland D 2001 *J. Chem. Phys.* **115** 7669
[10] Lucht R, Bahr Ch and Heppke G 2000 *Phys. Rev.* E **62** 2324
[11] Dietrich S and Haase A 1995 *Phys. Rep.* **260** 1
[12] Ohmasa Y, Kajihara Y, Kohno H, Hiejima Y and Yao M 2000 *J. Phys.: Condens. Matter* **12** A375
[13] See, e.g., Landau L D and Lifshitz E M 1958 *Statistical Physics* (New York: Pergamon) chapter 5 section 60
[14] Kajihara Y, Ohmasa Y, Kohno H, Hiejima Y and Yao M 2002 *J. Non-Cryst. Solids* **312–314** 489
Ohmasa Y, Kajihara Y and Yao M 2002 *J. Non-Cryst. Solids* **312–314** 472
[15] Yao M and Ohmasa Y 2001 *J. Phys.: Condens. Matter* **13** R297
[16] Kajihara Y 2003 *Doctoral Thesis* Kyoto University
[17] Hefner W 1980 *Doctoral Thesis* Marburg University
Hefner W, Schmutzler R W and Hensel F 1980 *J. Physique Coll.* **41** C8 62
[18] Pigeat P, Rouxel D and Weber B 1998 *Phys. Rev.* B **57** 9293 and references therein
[19] Nakanishi H and Fisher M E 1982 *Phys. Rev. Lett.* **49** 1565
[20] Nicolaides D and Evans R 1989 *Phys. Rev. Lett.* **63** 778
[21] Kellay K, Bonn D and Meunier J 1993 *Phys. Rev. Lett.* **71** 2607
[22] Ikezi H, Schwartzenegger K, Simons A L, Passner A L and McCall S L 1978 *Phys. Rev.* B **15** 2494
[23] Yao M, Takehana K and Endo H 1993 *J. Non-Cryst. Solids* **156–158** 807
[24] Tamura K *et al* 2002 *J. Non-Cryst. Solids* **312–314** 269
[25] Kohno H and Yao M 2002 *J. Phys.: Condens. Matter* **14** L171
[26] Inagaki T, Arakawa E T and Williams M W 1981 *Phys. Rev.* B **23** 5246
[27] Logan D E and Edwards P P 1986 *Phil. Mag.* B **53** L23
[28] Tarazona P and Evans R 1983 *Mol. Phys.* **48** 799
[29] Omata K and Yonezawa F 1998 *J. Phys.: Condens. Matter* **10** 9431
[30] Schick M 1990 *Liquids at Interfaces* (*Les Houches Session 48*) ed J Charvolin, J F Joanny and J Zinn-Justin (Amsterdam: North-Holland)
[31] Dietrich S 1988 *Phase Transitions and Critical Phenomena* vol 12, ed C Domb and J L Lebowitz (London: Academic) section 3